Synthesis of Some Metal Complexes with New Heterocyclic Ligand (5-(((2-(3-(1*H*-indol-3-yl)acryloyl)phenyl)amino)methylene)-2-thiooxodihydropyrimidine-4,6(1*H*,5*H*)-dione) and Their Biological Effectiveness as Antioxidant and Anti-Cancer

Thanaa Abdul Ameer Hilal and Ibtihal Kadhim Kareem*

Department of Chemistry, Faculty of Education for Girls, Kufa University, Najaf 54001, Iraq

* ***Corresponding author:***

email: ibtihal.dosh@uokufa.edu.iq

Received: April 26, 2024
Accepted: September 10, 2024

DOI: 10.22146/ijc.95731

Abstract: *A novel ligand 5-(((2-(3-(1*H*-indol-3-yl)acryloyl)phenyl)amino)methylene)-2-thioxodihydropyrimidine-4,6(1*H*,5*H*)-dione) (L_1) which contains two groups of carbonyl synthesized in one pot and three-component reaction with thiobarbituric acid as starting material, and its complexes with Co(II), Ni(II), Cu(II), Zn(II) and Au(III) have been synthesized. The results of spectrophotometry, nuclear magnetic resonance of proton (H-NMR), infrared spectroscopy (FTIR), ultraviolet and visible (UV-vis) spectroscopy, X-ray diffraction (XRD), elemental analysis (CHNS) and molar conductivity measurements were used to suggest the proposed structures. These data have been utilized to propose appropriate geometric configurations for all complexes. The L_1 coordinates toward the metal ions Co(II), Ni(II), Cu(II), and Zn(II), giving an octahedral geometry, while it has a square planar shape with the Au(III) ion. Scanning microscopy (FE-SEM) was used to determine the size of nanoparticles. The present investigation employs a comprehensive molecular docking analysis to assess the binding energies of anti-cancer drugs, thereby elucidating their binding affinity towards the receptor. This indicates that the $[Au(L_1)Cl]Cl_2$ complex has a strong affinity for the protein kinase (1HK7). Significant antiproliferative activity was seen in it against human breast cancer (MCF-7) and normal cell lines (MCF-10), as evidenced by the IC_{50} and selective indices (SI) values. This study could contribute to the development of pharmaceutical preparations.*

Keywords: *thiobarbituric acid derivatives; X-ray diffraction; MCF-7; nano metal complexes; molecular docking study*

■ INTRODUCTION

Indole (1*H*-benzo[b]pyrrole) is a widely occurring heterocyclic structure in both naturally derived and synthetically produced bioactive compounds. A key feature of the indole scaffold is its ability to interact with various receptors [1], influencing a broad spectrum of biological activities. Consequently, indole derivatives exhibit a series of biotic effects and are currently utilized to treat numerous medical conditions [2]. Pharmaceuticals containing an indole moiety and approved for therapeutic use include zafirlukast (used for asthma), pindolol (used for lowering blood pressure), indomethacin (used for inflammation), roxindole (used for psychosis), sumatriptan (used for migraines), and arbidol (used for antiviral) [3-5].

The indole scaffold has proven to be a highly valuable motif in the development of cancer treatments, particularly those effective against both drug-resistant and non-drug-resistant types of cancer [2,6]. As cancer tumors increasingly exhibit resistance to conventional chemotherapy, the exploration of alternative treatment strategies, including the development of novel agents targeting drug-resistant cancers, becomes essential [7-9]. The MCF-7 cell line, which has estrogen receptors, serves as a useful experimental model for studying hormone-regulated genes, as certain proteins are induced in response to estrogen [10]. Cancer of breast, existence the most predominant cancer type amongst females, underscores the urgent need for promising, targeted anti-cancer therapies in modern oncology [11].

Hence, there is a pressing want for promising, targeted anti-cancer medications in contemporary oncology.

Chemotherapy is a primary treatment modality for cancer patients, and many tumors initially respond well to chemotherapy drugs from a clinical perspective. Our ongoing research on biologically active heterocyclic compounds has highlighted the significant roles of indole, which exhibits a range of biological activities, including antimicrobial, anti-HIV, and antifungal effects [12-13]. Recent literature has also revealed the anti-cancer potential of indole derivatives. For instance, derivatives of 2-phenyl-1*H*-indole-3-carbaldehyde have been shown to efficiently prevent the propagation of MCF-7 cells by integrating barbituric acid and indole moiety. Additionally, novel hybrid compounds have been synthesized and evaluated for their potential as anti-cancer agents [14]. Chalcone, another key structural motif in many natural and synthetic compounds, has been recognized for its broad pharmacological effects. Over the past few decades, various chalcone derivatives have demonstrated significant anti-cancer properties, particularly through their ability to interfere with the polymerization or depolymerization of tubulin [15].

Various forms of barbituric acid products possess a variety of bio-effectiveness, such as anticonvulsant, anti-HIV, and antibacterial effects. They are also known to inhibit cyclin-dependent kinase-2 and tyrosine kinase, both of which are crucial for cell cycle regulation and signal transduction. Among these derivatives, 5-benzylidene thiobarbituric acid and 5-benzylidene-4,6-pyrimidinediones have shown superior efficacy as tyrosine kinase inhibitors and antibacterial agents [16-17].

Indoles are of wide interest in the medical field as therapeutic compounds, where complexes of Au(III), Co(II), and Cu(II) have been prepared with the ligand (*N*-(2-((*E*)–(4,5-diphenyl-1*H*-imidazol-2-yl)dibenzyl)-1-(1*H*-indol-3-yl)methanimine) derived from indole and studying its biological effects as antioxidants, as it proved to be highly effective as a good therapeutic agent. The effect of the complex of Au(III) on MCF-7 cells was studied and also compare with MCA-10 healthy cells, as it showed high efficiency in inhibiting MCF-7 cancer cells while remaining safe for cells. Intact MCA-10, and thus these complexes can be considered as therapeutic agents with high efficiency and selectivity for the cancer cells after conducting more comprehensive studies [18].

Our study aims to synthesize and characterize a novel heterocyclic ligand (L_1) derived from thiobarbituric acid (TBA) and investigate its transition metal complexes. Spectroscopic analysis and bioassay evaluation of these complexes against a breast cancer cell line were performed. In addition, molecular docking studies have been performed to evaluate their effectiveness as drugs for the mentioned type of cancer and potential antioxidants.

■ EXPERIMENTAL SECTION

Materials

The materials used in this study are indole-3-carboxaldehyde, 2-aminoacetophenone, TBA, trimethyl orthoformate, and silver nitrate, which were purchased from Sigma Aldrich, England. $CoCl_2{\cdot}6H_2O$, $NiCl_2{\cdot}6H_2O$, $ZnCl_2$, $CuCl_2{\cdot}2H_2O$, ethanol, methanol, and sodium hydroxide were from B.D.H Company. Benzene was obtained from G.C.C. company while hydrogen tetrachloroaurate(III) trihydrate was obtained from Glentham Life Sciences. Ethanol absolute was from Sharlut company. Dimethyl sulfoxide (DMSO) was purchased from A.C.S. company. All these chemicals were utilized without extra purification as they are equipped.

Instrumentation

Melting point measurements for L_1 and its complexes were done by using electrothermal 9300 melting point LTD from UK. Proton nuclear magnetic resonance spectra were acquired as solutions in DMSO-d_6 solvent by applying 500 MHz to a Varian spectrophotometer. For UV-visible spectra, a Shimadzu spectrophotometer with dual-band model 1700 was used. A Shimadzu FTIR 8400 spectrometer utilizing KBr particles in the 4000–400 cm^{-1} wavelength range was using for measured FTIR spectra. A fine analysis of carbon, hydrogen, and nitrogen elements was performed using a C.H.N elemental analyzer (EURO 2012EA 300). Used field emission scanning electron scanning device (FESEM) was used to take a very magnified image of the large

magnification (20.00 kX) of the device for the eyes to use (ZEISS EM 3200, Germany), Bestic Aluminum anode from Germany was used for recording X-ray diffraction. Biohazard safety cabinet class (II) BGenex (USA), autoclave Arnold Sons (USA), centrifuge Hermle (Germany), cell culture incubator (Memmert, Germany), deep freezer (−800 °C) from Marubeni, Japan, cooling centrifuge (Beckman Model J2-21, USA), distillatory Ogawa Seiki (Japan), drying and sterilization oven (Hermle, Germany), incubator Memmert (Germany), ELISA reader (Organon Teknika), inverted microscope (Leica, Germany), multiwall plate, microtiter plate, and 96-well plate from USA were used. The pH-meter (LKB, Sweden), millipore filter (0.22 μm) from Sartorius, Germany, sterile tissue culture flasks (25.75 cm^2) from Nunc, Denmark, water bath (Memmert, Germany), and vacuum pump (Leitz, Germany) were used.

Procedure

Preparation of L_1

The L_1 is prepared in two steps: the first step is preparing the chalcone compound 1-(2-aminophenyl)-3-(1*H*-indol-3-yl)prop-2-en-1-one (B_1) by using the Claisen-Schmidt condensation method, where 2 g (0.0137 mol) indole-3-carboxaldehyde was reacted with 1.84 g (0.0137 mol) of 2-aminoacetophenone. An amount of 5 mL 10% NaOH was added by stirring with a magnetic stirrer for 8 h.

The second step is preparing L_1 by reacting 0.864 g (0.006 mol) of TBA and mixed with 1.5 mL (0.0125 mol) of trimethyl orthoformate [19]. With a magnetic stirrer, the mixture was heated and stirred for 5 h, then 10 mL of EtOH absolute was added to the mixture, and 1.305 g (0.005 mol) of B_1 was added to the intermediate compound. Then, the reaction was heated for 8 h. The yellow precipitate was recrystallized from ethanol and dried. The percentage of the new ligand that resulted was 90%, with a melting point value 195 °C. Scheme 1 shows the steps for preparing the new ligand.

General synthesis of metal complexes

As much as 0.166 g L_1 (0.0004 mol) was mixed with a 10 mL absolute ethanol to produce the nano-metal complexes to 0.0475 g (0.00024 mol), each of $CoCl_2{\cdot}6H_2O$,

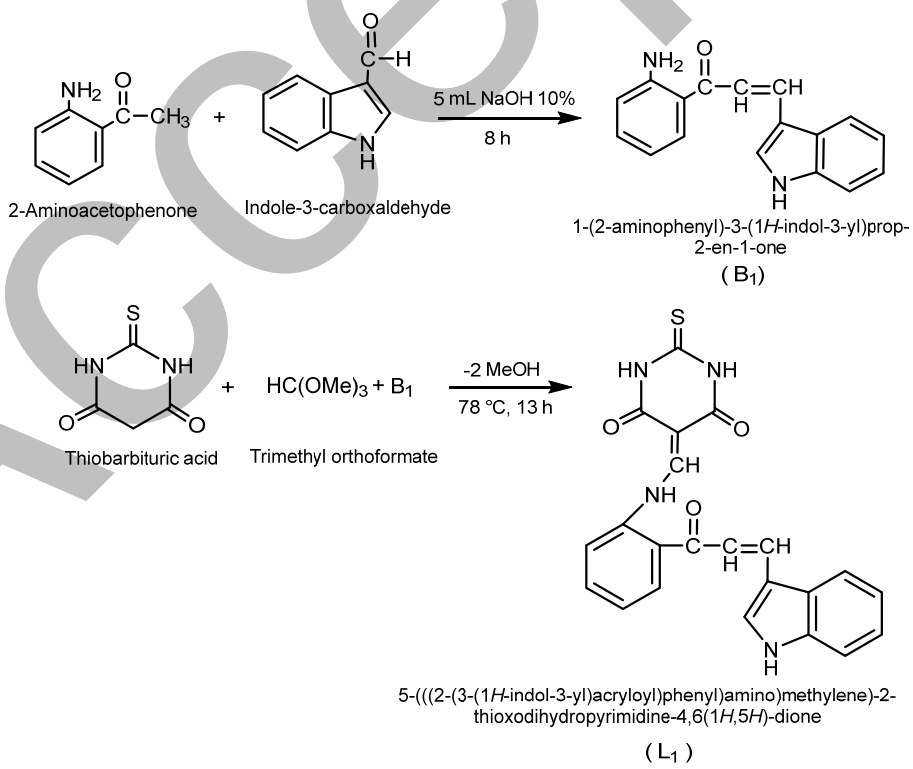

Scheme 1. The steps for preparing L_1

$NiCl_2{\cdot}6H_2O$ and $CuCl_2{\cdot}2H_2O$ respectively and 0.0272 g (0.00024 mol) for $ZnCl_2$ in 10 mL absolute ethanol solution of molar ratio (1 metal:2 ligand). The solutions were refluxed for 2 h, and precipitated complexes were obtained by decreasing the volume using evaporation. The complexes were subjected to vacuum drying.

Preparation of nano-gold complex $[AuL_1Cl]Cl_2$

The preparing of $[AuL_1Cl]Cl_2$ complex includes adding 0.095 g (0.0024 mol) of $NaAuCl_4{\cdot}2H_2O$ in 10 mL absolute ethanol solution of 1:1 (metal: ligand) molar ratio to 0.1 g (0.00024 mol) of L_1, after adding 10 mL of acetonitrile to the solution. The resulting solution was refluxed for 25 h and a precipitated complex was obtained through an evaporation method. The complex was subjected to vacuum drying. The complexes physical parameters are being investigated, as presented in Table 1. Scheme 2 provides a visual representation of the stages involved in the synthesis of metal complexes.

In vitro *cell cytotoxicity and viability assays*

Development of breast cancer cell line (MCF 7-cells). To prepare cancerous and healthy cell lines for study. The MCF-7 cell line, sourced from human breast cancer, was obtained from the National Cell Bank of Iran at the Pasteur Institute and treated according to the procedure [11]. The cells were cultured in RPMI-1640 medium (Gibco) supplemented with 10% fetal bovine serum and treated with antibiotics (100 U/mL penicillin and 100 µg/mL streptomycin). The cells were maintained at 37 °C in a humidified environment with 5% CO_2. Trypsin/EDTA (Gibco) and a phosphate-buffered saline (PBS) solution were utilized for cell transfer. The 3-(4,5-dimethylthiazol-2-yl)-2,5-diphenyltetrazolium bromide (MTT) assay was used to assess cell proliferation and viability. For monolayer culture, the cells were treated with trypsin to dissociate them, collected, and adjusted to a density of 1.4×10^4 cells per well. They were then seeded

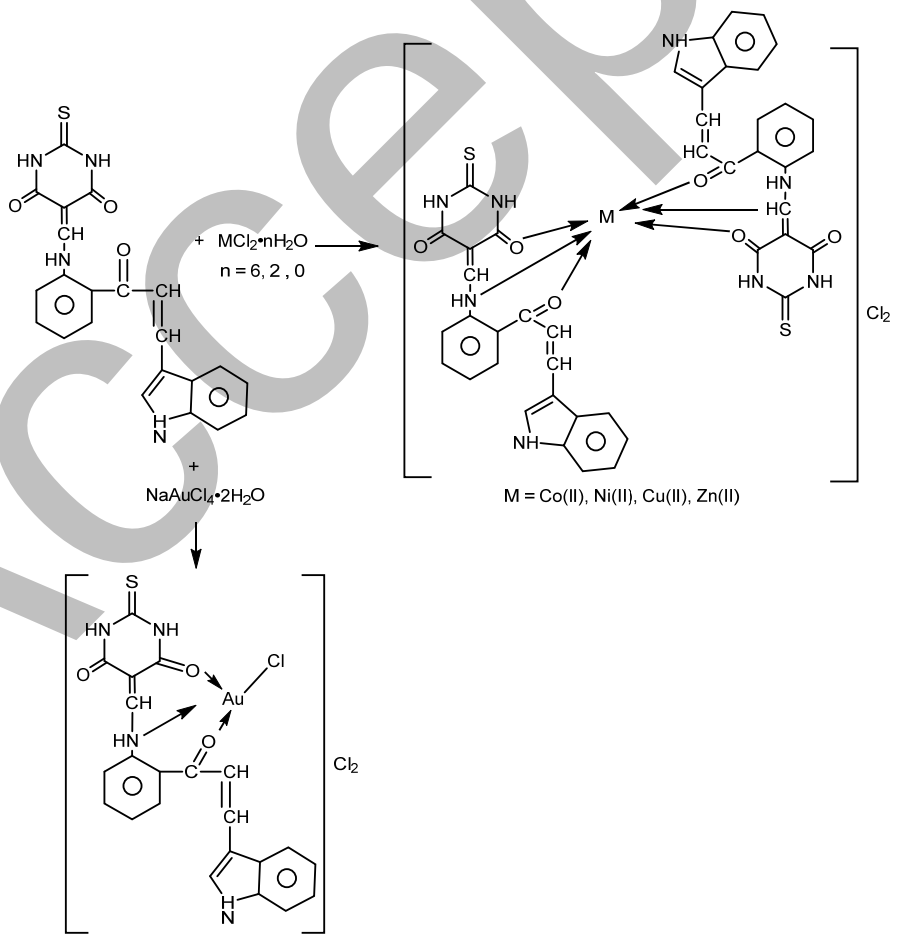

Scheme 2. The procedure of synthesis of nano-metal complexes of L_1

into 96-well plates containing 200 µL of fresh media per well and incubated for 24 h to allow for single-layer formation. Once established, each hole was filled with a cell suspension, and then a specific concentration of $[AuL_1Cl]Cl_2$ complex (7.40, 22.22, 66.66, 200.00, 600.00 µg/mL) was added to the holes for 48 h at 37 °C in a 5% CO_2 environment. There were three holes for each concentration. After the 24 h treatment, the monolayer culture was left undisturbed in the original plate. The liquid above the culture was carefully removed, and 200 µL of MTT solution (0.5 mg/mL in PBS) was added to each well. The plate was then incubated at 37 °C for an additional 4 h. Following this incubation, 100 µL of DMSO was added to each well to dissolve the formazan crystals formed by the MTT assay. The plate was shaken at 37 °C to ensure complete dissolution. Absorbance was measured at 570 nm using an ELISA reader (Model Wave xs2, BioTek, USA). The IC_{50}, representing the concentration of the compounds that induced 50% cell death, was calculated from the dose-response curves.

Antioxidant activity

The *in vitro* antioxidant activity of the synthesized complexes was evaluated by using the 1,1-diphenyl-2-picrylhydrazyl (DPPH) assay. Stock solutions of the drugs were prepared in methanol at concentrations ranging from 50 to 200 mg/mL [20]. The amount of 2 mL of synthesized compounds was mixed with 1 mL of DPPH solution in methanol with a concentration of 0.003% w/v. The solution was briskly agitated and then left for 30 min. The absorbance was measured at 517 nm to determine the extent of free radical scavenging. Ascorbic acid was used as the reference standard. The percentage of inhibition (I%) was calculated using Eq. (1);

$$I\% = \frac{A_c}{A_c - A_s} \times 100\% \quad (1)$$

where A_c is the absorbance of the control and A_s is the absorbance of the sample.

■ RESULTS AND DISCUSSION

Excellent solubility in different solvents was tested for metallic complexes such as DMF, DMSO, MeOH, and EtOH. Additionally, they exhibit stability in the presence of air. These metal complexes and the ligand were studied using various analytical methods, including fine analysis of elements (Table 1), molar electrical conductivity, infrared, UV-vis, mass spectrum measurement, and NMR (only ligand measured). The experimental results and analytical data of the complexes are in good agreement, confirming their accuracy. Based on the data shown in Table 1, specifically, the results of precise element analysis (CHNS) and molar conductivity measurements were adopted molar ratio was 1:2 (M:L) of the complexes Co(II), Ni(II), Cu(II), and Zn(II) where the tridentate ligand coordinates with metal ions through

Table 1. The element analysis of the new heterocyclic ligand (L_1) and its metallic complexes and some tangible properties

Formula	Found calc. (%)				M.Wt	Color	M.P °C	Yield (%)
	C	H	N	S				
(L_1) = $C_{22}H_{16}N_4O_3S$	63.4615 63.9761	3.8461 4.2341	13.4615 13.9873	7.6923 8.4532	416.00	Yellow	195–198	90
$Co[(C_{22}H_{16}N_4O_3S)_2]Cl_2$	54.8970 55.4532	3.3270 3.7756	11.6448 11.9871	6.6542 7.4352	961.80	Brown	240 decompose	85
$[Ni(C_{22}H_{16}N_4O_3S)_2]Cl_2$	54.9090 55.3440	3.3278 3.8762	11.6473 11.9986	6.6556 6.8984	961.59	Yellow	235 decompose	88
$[Cu(C_{22}H_{16}N_4O_3S)_2]Cl_2$	54.6357 54.9782	3.3112 3.9564	11.5894 11.9880	6.6225 7.3230	966.40	Reddish brown	200 decompose	84
$[Zn(C_{22}H_{16}N_4O_3S)_2]Cl_2$	54.5296 54.9876	3.3048 3.7865	11.5669 11.8773	6.6096 7.3221	968.28	Orange	238 decompose	89
$[Au(C_{22}H_{16}N_4O_3S)Cl]Cl_2$	36.7023 37.4432	2.2243 2.7652	7.7853 8.3210	4.4487 4.9650	719.30	Brown	165	80

3 sites (NNO) to form an octahedral shape, while in the gold complex, the tridentate ligand coordinates with Au(III) ion through the coordination sites mentioned above to take square planar geometry. Thus, the surrounding ligands coordinate around the core metal ions. This aligns with what has been mentioned in previous literature regarding this type of complex [21-22]. The chelate complexes synthesized in this study exhibited significant conductivity levels, demonstrating that complexes exhibit an electrolytic character.

^{1}H-NMR Spectra

The chemical surroundings of organic molecules may be determined via NMR spectroscopy, using tetramethylsilane (TMS) as the internal reference standard [23]. The L_1 was analyzed using the ^{1}H-NMR technique with DMSO-d_6 as the solvent (Fig. S1(a)). The spectrum obtained provided reliable data, and the molecular structure was determined based on the chemical shift of the hydrogen atoms. The spectrum exhibited distinct signals, including a signal singlet at 2.5 ppm corresponding to the solvent protons [24], and a signal singlet at 8.58 ppm attributed to the C–H group of the indole ring. It also showed doublet signals at 8.31 ppm dating back to the CH proton in the (CH–NH) group. Also, a singlet signal appeared at 8.13 ppm, dating back to CH=CH group, and the ligand showed a singlet signal at 8.23 ppm belonging to the proton of the O=CH group. Likewise, a singlet signal appeared at 9.96 ppm belonging to the proton N–H in the NH–CH group, as the ligand showed. A singlet signal appeared at 10.5 ppm that belongs to the proton of the H–N group in the indole ring. Likewise, a singlet signal appeared at 13.6 that refers to the N–H proton of the thiobarbituric acid ring. The ligand also showed multiple signals ranging from 6.37–7.57 ppm that belong to the protons of aromatic ring multiples signals. As for the zinc complex ($[Zn(L_1)_2]Cl_2$), it showed signals very similar to those of the ligand, as shown in Fig. S1(b).

FTIR Spectra Studies of L_1 and Its Metal-Complexes

The spectra of the complexes were compared with the spectrum of the free ligand to identify any alterations that may have occurred during the complexation process. FTIR spectra showed important and distinctive domains in the chemical structure of L_1 ligands and complexes that confirm the formation of complexes. A change was observed in some important bands in the spectra of the complexes, such as C=O and C–N. It suffered from changes in the location, intensity, and shape of the beams. Other new bands in the range of 400–700 cm^{-1} refer to the formation of M–N and M–O bond types, which indicate coordination between metal and ligand L_1 through the indicated sites coordination with metals by this group in this way inspired by previously published articles [25-26]. All relevant data can be found in Table 2, Fig. S2(a–f), which shows the infrared spectra of the prepared ligand and its complexes.

Measurement of Molar Conductivity

The results show that the investigated chelate complexes of ions had molar electrical conductivities ranging from 85.5 to 121.2 S cm^2/mol when measured in solutions with the novel ligand and a concentration of 1×10^{-3} M per complex. These measurements were conducted at laboratory temperature and DMSO was used as the solvent. The specific values are listed in Table 3.

Table 2. The infrared (IR) spectrum frequencies for the new heterocyclic ligand and associated metal complexes

Compound	ν(N–H) (cm^{-1})	ν(C=C) (cm^{-1})	ν(C=O) (cm^{-1})	ν(HC=C) alkene (cm^{-1})	ν(C–H) aromatic (cm^{-1})	ν(C=S) (cm^{-1})	ν(M-O) (cm^{-1})	ν(M–N) (cm^{-1})
Ligand (L_1)	3448	1580	1631	3169	3107	1130	---	---
$[Co(L_1)_2]Cl_2$	3464	1600	1639	3182	3108	1134	439	574
$[Ni(L_1)_2]Cl_2$	3464	1608	1639	3182	3100	1135	425	570
$[Cu(L_1)_2]Cl_2$	3446	1590	1638	3172	3105	1138	414	536
$[Zn(L_1)_2]Cl_2$	3464	1610	1641	3182	3108	1138	440	572
$[Au(L_1)_2]Cl_3$	3435	1583	1638	3170	3100	1132	440	559

Table 3. The complexes' molar conductivities

Complex	S cm^2 mol^{-1}
$[Co(L_1)_2]Cl_2$	97.1
$[Ni(L_1)_2]Cl_2$	105.1
$[Cu(L_1)_2]Cl_2$	85.5
$[Zn(L_1)_2]Cl_2$	91.6
$[Au(L_1)Cl]Cl_2$	121.2

We can observe the ionic properties of all these complexes from these measurements. The results are consistent with the findings reported in the literature for metallic compounds with ionic characteristics [27].

Electronic Spectra

Electronic absorption spectra are valuable for assessing the impacts facilitated through alternative methods of structural investigation. The L_1 spectrum in DMSO as a solvent exhibited three absorption peaks: at 264 and 295 nm corresponding to electron transitions of the $\pi \rightarrow \pi^*$ type, and at 455 nm attributed to an electron transition of the $n \rightarrow \pi^*$ type. The presence of double bonds in the ligand, which are connected to atoms with unshared electron pairs, caused this third peak to be consistent with what was reported by Radhi et al. [28].

The ligand spectrum was compared to that of the Co(II) complex, which exhibited an absorption peak at a wavelength of 439 nm due to metal-ligand charge transfer (MLCT) and an absorption peak at 463 nm has been attributed to the electron transition $\nu_2 = {}^4T_1g_{(F)} \rightarrow {}^4T_1g_{(P)}$. Absorption peak which showed at 530 nm has been suggested as a result of electron transfer $\nu_1 = {}^4T_1g_{(F)} \rightarrow {}^4T_1g_{(F)}$. This observation aligns with the existing research on the occurrence of this band in Co(II) complexes octahedral geometry [29]. The Ni(II) complex spectrum solution shows an absorption peak at 388 nm due to charge transfer M→L, CT, while the absorption peak was detected at 463 nm due to electron transition $\nu_3 = {}^3A_2g_{(F)} \rightarrow {}^3T_1g_{(P)}$, Well a pack appeared at 576 nm due to electron transition $\nu_2 = {}^3A_2g_{(F)} \rightarrow {}^3T_1g_{(F)}$, and this supports with the literature on Ni(II) complexes octahedral geometry [22,28].

The spectrum of Cu(II) complex presented an absorption peak at 440 nm that was attributed to electron transition $\nu_3 = {}^2B_1g \rightarrow {}^2Eg$ and a broad absorption peak at 463 nm due to the electron transition $\nu_2 = {}^2B_1g \rightarrow {}^2B_2g$, and pack appeared at 630 nm due to the electron transition $\nu_1 = {}^2B_1g \rightarrow {}^2A_1g$, this is consistent with what was mentioned in the literature [30].

The Zn(II) complex spectrum presented an absorption peak at 465 nm due to MLCT. As for the electronic spectrum, the Au(III) complex with L_1 ligand. This complex exhibited one band at 538 nm, which was assigned to the ${}^1A_1g \rightarrow {}^1B_1g$ transition. The Au(III) complex has a diamagnetic moment and square planar geometry. Recently, complexes of Au(III) ions have been used in medical fields to treat cancer. Its importance has significantly increased in this field. The reason is that Au(III) is electronically identical to Pt(II), and the Au(III) complexes, which are tetra-symmetric and have a square planar shape, are similar to cisplatin in electronic arrangement and geometric shape, or both. The fact that Zn(II) and Au(III) complexes have five full d orbitals means they don't have d-d electronic transmissions. The emergence of additional peaks in the metallic complexes, which were not present in the ligand spectrum, suggests that the metallic complexes were in line with the ligand, likely due to charge transfer [31]. The red shift in complexes is caused by the transfer of charges from the ligand to the metal (LMCT). Table 4 lists the electronic spectra of L_1 and its complexes in DMSO solvent. Fig. S3(a–c, and e) shows the electronic spectra of the prepared ligand and its metallic complexes.

FESEM of Complexes

FESEM technology offers a flexible approach to analyzing the surface morphology (shape and size of particles) and topography (surface properties) of substances [32-34]. Prior to imaging, a thin layer of material with a 15 kV acceleration voltage, a 200 nm cross-sectional distance, and a 135 kX magnification force was applied to the samples. Fig. 1 shows the crystalline agglomeration of the metal complexes, as observed in the FESEM images. Particle sizes were calculated using Image J software.

The micrograph of the $[Au(L_1)Cl]Cl_2$ complex reveals particles with irregular shapes and an average size

Table 4. The electronic spectra of L_1 and its metallic complexes in DMSO solvent

Compound	λ (nm)	Transition	Geometry	Hybridization
	264	π→π*		
L_1	295	π→π*	---	---
	455	n→π*		
	530	$^4T_1g_{(F)}\rightarrow{}^4T_2g_{(F)} = \nu_1$		
$[Co(L_1)_2]Cl_2$	463	$^4T_1g_{(F)}\rightarrow{}^4T_1g_{(P)} = \nu_2$	Octahedral	sp^3d^2
	439	M→L, CT		
	576	$^3A_2g_{(F)}\rightarrow{}^3T_1g_{(F)} = \nu_2$		
$[Ni(L_1)_2]Cl_2$	463	$^3A_2g_{(F)}\rightarrow{}^3T_1g_{(P)} = \nu_3$	Octahedral	sp^3d^2
	388	M→L, CT		
	630	$^2B_1g\rightarrow{}^2A_1g = \nu_1$		
$[Cu(L_1)_2]Cl_2$	463	$^2B_1g\rightarrow{}^2B_2g = \nu_2$	Octahedral	sp^3d^2
	440	$^2B_1g\rightarrow{}^2Eg = \nu_3$		
$[Zn(L_1)_2]Cl_2$	465	M→L, CT	Octahedral	sp^3d^2
$[Au(L_1)Cl]Cl_2$	538	$^1A_1g\rightarrow{}^1B_1g$	Square planar	dsp^2

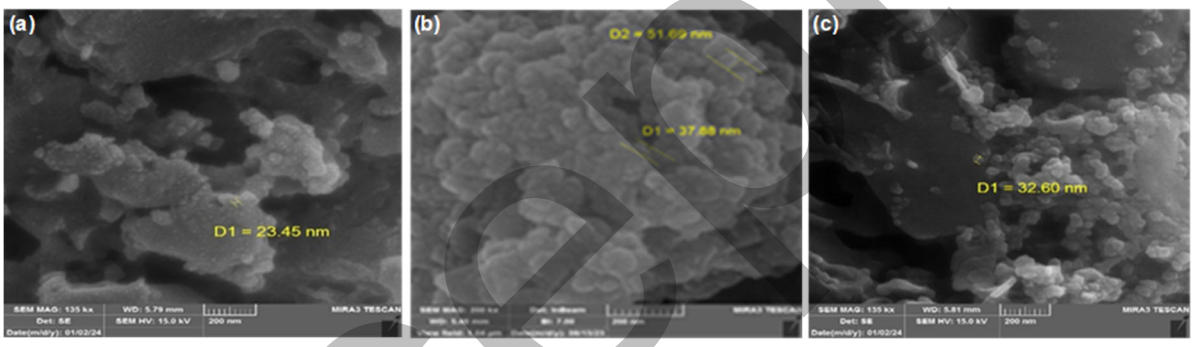

Fig 1. FESEM images for (a) Zn(II), (b) Cu(II) and (c) Au(III) complexes

of 40.62 nm. The Cu(II) complex exhibits a non-uniform size distribution, with an average particle size of 32.60 nm. In addition, the Zn(II) complex consists of particles with an average size of 23.45 nm. These particles have a non-uniform and irregular morphology and an average particle size of less than 100 nm, which indicates that they are nanomaterials. The coordination sphere and geometric layout of the complexes may vary depending on the chemical nature of the ligand [35]. Ultimately, this leads to markedly distinct physical forms [36-37]. The FESEM micrographs of the complexes exhibit significant variation due to the coordination of metal ions with donor sites. The images reveal that the grain sizes of the synthesized compounds are smaller than 100 nm, placing them within the nanoscale range. This increased surface area enhances the quantitative effect, creating new energy levels that allow electrons to move more freely. The properties of the ligand and its complexes make them promising candidates for medical research, particularly in the study of their potential to inhibit various types of cancer [21].

XRD

XRD provides precise data regarding solid-state materials' molecular or atomic configuration [38]. The XRD diffractograms were measured for L_1 and $[Au(L_1)Cl]Cl_2$. The calculation of CuKα radiation was performed in the 2θ range of 0° to 80°, with a wavelength of 1.54060 Å and generator settings of 30 mA/40 kV. Using the Xpert High Score computer program, various parameters of diffraction spectra can be measured by analyzing the identified peaks [39]. The results indicated that the compounds exhibited a semicrystalline character, as depicted in Fig. S4(a and b). By applying

Bragg's equation [40], we estimated the significant reflections and measured the corresponding d-spacing values. The equation $n\lambda = 2d \sin\theta$ was used, where d represents the distance between the crystalline layers and n is an integer (1, 2, 3, ...). The symbol λ represents the wavelength of X-ray CuKα, which is 1.540598 Å. The symbol θ represents the diffraction angle. The equation developed by Debye and Scherrer was utilized to ascertain the average diameter of the crystallite as well as its size distribution (Eq. (2)) [41];

$$D = k\lambda/\beta\cos\theta \quad (2)$$

where D represents the average diameter of the crystallite, k is the shape factor (0.891) and β is the line broadening at half the maximum intensity (FWHM) [42]. The X-ray spectra showed a clear difference in the previously mentioned data, including the spacing between the crystalline levels (d), the crystal size (D), the microductility (ε), and the density of dissolutions (δ). This confirms the occurrence of the coordination process. Between the prepared ligand and its metal complexes under study, we noticed that there is an inverse proportion between D, ε, and δ, as the greater D, the lower ε and the lower δ, and thus the crystal defects decrease. The sharp peaks indicate crystalline or semi-crystalline structures. The intensity of these peaks depends on the crystal arrangement, the properties of the crystal lattice, and the crystal planes. In addition, The experimental average sizes for L_1 and peak radian of the reported $[Au(L_1)Cl]Cl_2$ were 13.7117 and 36.3281 nm, respectively. These compounds exhibit nanostructural properties, as evidenced by their crystalline size, having a particle size of less than 100 nm [43].

These obtained data support our previous measurements of FESEM analyses. The crystalline properties of ligand L1 and the Au(III) complex can be found in Table 5 and Fig. S4(a and b) represent the XRD spectra of ligand L_1 and its nano Au(III) complex.

Molecular Docking

A molecular docking study can offer a more comprehensive understanding of how novel drugs exhibit bioactivity against a target by determining the modalities of interaction and binding affinities [44]. A docked complex conformation, chosen based on prior investigations [45] and docking scores, was assessed for

Table 5. The crystallographic parameters for L_1 and its nano-complex

Compounds	Position (2θ (°))	Height (cts)	FWHM (2θ (°))	d-spacing (Å)	Relative intensity (%)	Tip width (2θ (°))	D (nm)
L_1	10.7441	209.3800	0.5904	8.23450	22.0300	0.7085	
	12.5753	412.1000	0.5904	7.03923	43.3500	0.7085	
	16.3002	786.3900	0.5904	5.43805	82.7200	0.7085	
	19.4367	877.8500	0.5904	4.56703	92.3500	0.7085	
	22.2391	420.7300	0.5904	3.99746	44.2600	0.7085	13.7117
	24.0952	486.6800	0.5904	3.69357	51.2000	0.7085	
	28.4815	950.6100	0.5904	3.13393	100.0000	0.7085	
	32.3887	430.5600	0.5904	2.76424	45.2900	0.7085	
	33.6262	440.3200	0.5904	2.66529	46.3200	0.7085	
	38.0555	285.7800	0.5904	2.36465	30.0600	0.7085	
$[Au(L_1)Cl]Cl_2$	12.6676	137.5300	0.5904	6.98813	14.4300	0.7085	
	16.3067	208.8200	0.1476	5.43592	21.9000	0.1771	
	19.5541	213.9600	0.2952	4.53988	22.4400	0.3542	
	28.6997	212.8900	0.2952	3.11060	22.3300	0.3542	
	29.6011	953.3300	0.1968	3.01790	100.0000	0.2362	36.3281
	32.1090	300.1200	0.1476	2.78768	31.4800	0.1771	
	39.1727	461.0600	0.1968	2.29974	48.3600	0.2362	
	48.0859	226.1800	0.2400	1.89067	23.7300	0.2880	

Table 6. Effect of the complex $[Au(L_1)_2]Cl_3$ on MCF-7 and their comparison with MCF-10A by using the MTT test for 24 h at a temperature of 37 °C for the same concentration

Concentration (μg/mL)	Mean percentage for each cell line (%)			
	Cancerous line cells of MCF-7		Normal line cells of MCF-10A	
	Cell viability	Cell inhibition	Cell viability	Cell inhibition
7.40	95.20	4.80	94.33	5.67
22.22	90.15	9.85	81.38	18.62
66.66	64.84	35.52	76.70	23.30
200.00	22.31	77.69	53.20	46.80
600.00	21.13	78.87	52.78	47.22
	IC_{50}= 103.43		IC_{50} = 566	

its binding interactions with the breast cancer protein (PDB ID: 1HK7). Tables 5 and 6 demonstrate that the docking investigation revealed the presence of non-covalent interactions, including π-cation, π-ionic, π–π, and hydrogen bonding interactions, in the produced compounds. The docking score values of all the compounds showed excellent outcomes with the protein. In general, a lower energy value (S) indicates greater stability of the docking site and stronger interaction between the docking site and protein receptor [46]. Table 6 displays the atom locations' binding free energy docking scores (S) and root-mean-square deviations (RMSD). The binding score of the Au(III) metal complex to the 1HK7 protein was predicted to be −6.5053 kcal/mol. Therefore, In terms of the coordination pattern, the Au(III) complex formed one H-donor bond and three H-acceptor bonds in 1HK7 protein via sulfur 1, and arene-H with ASN 405 (A), LYS441 (B), LYS 441 (A), all with bond distances of 3.65–4.35 Å. The 2D, 3D, and map interactions for the target are illustrated in Fig. 2.

Proposed Structure

The results reached the octahedral shape of the nano-complexes of Co(II), Ni(II), Cu(II) and Zn(II)) while the square planar shape was proposed for the gold complex with L_1 (Fig. 3).

Anti-Cancer Screening (*In Vitro* Cytotoxicity)

The impact of Au(III)-complex on the proliferation of cancer cell lines (MCF-7) and healthy cells (MCF-10A)

The data presented in Table 7 demonstrates the impact of the compound $[Au(L_1)Cl]Cl_2$ on the proliferation of the MCF-7 cell lines and normal MCF-10A cells. The highest inhibition of $[Au(L_1)Cl]Cl_2$ complex for MCF-7 was 78.87% at 600 μg/mL, while the

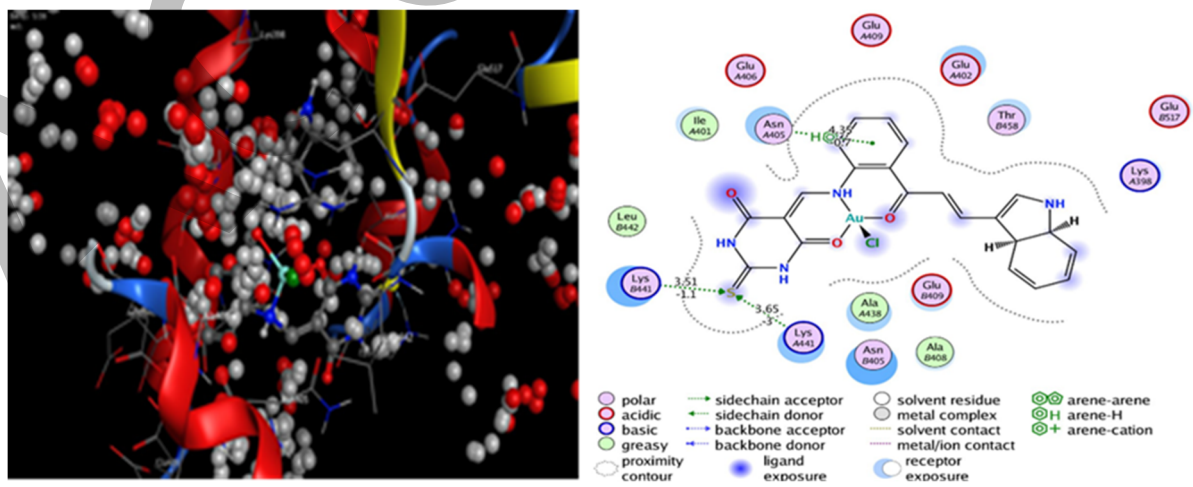

Fig 2. The 2D and 3D views of intermolecular interactions of $[Au(L_1)Cl]Cl_2$ complex with 1HK7 protein

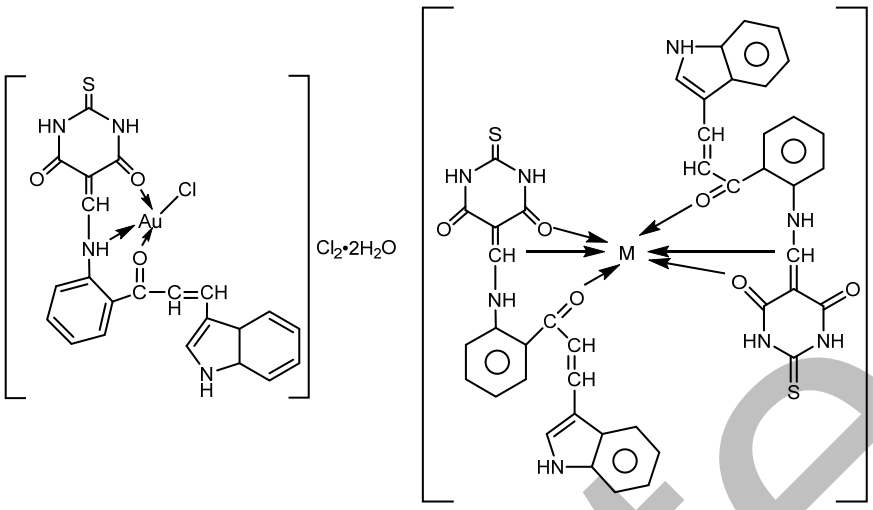

Fig 3. Proposed structure of the metallic complexes

Table 7. Scavenging activity of some synthetic compound

DPPH scavenging activity (%)					
Concentration	Ascorbic acid	L_1	$[Au(L_1)Cl]Cl_2$	$[Zn(L_1)_2]Cl_2$	$[Cu(L_1)_2]Cl_2$
200.0	79.03333	81.09533	58.25600	49.46000	66.82100
100.0	74.06667	69.48300	50.34700	40.54800	50.19300
50.0	64.26667	55.24700	42.55400	31.63600	40.35500
25.0	54.66667	44.29033	29.82233	17.12967	25.50167
12.5	36.23333	29.12833	21.79800	14.15900	16.08800

lowest inhibition percentage was 5.67% at the concentration of 7.4 µg/mL for MCF-10A cells of the complex. The results also showed that the best percentage of inhibition of $[Au(L_1)Cl]Cl_2$ complex for the MCF-7 cancer and MCF-10A healthy cell lines is at 7.4 µg/mL. Where it was observed that the half-inhibitory concentration of the complex $[Au(L_1)Cl]Cl_2$ in the cells of the MCF-7 cell line equals (103.43 µg/mL), which is very low compared to the half-inhibitory concentration of the cells of the healthy line, equal to 566 µg/mL. This is an excellent result because we need a very high concentration to kill half of the healthy cells, and this result indicates the possibility of using the complex $[Au(L_1)Cl]Cl_2$ as a new treatment against this type of cancer. Table 6 shows the effect of the complex $[Au(L_1)Cl]Cl_2$ on MCF-7 and their comparison with MCF-10A for the same concentration using the MTT test for 24 h at 37 °C. Fig. S5(a and b) show the half inhibitory concentration of MCF-7 and MCF-10. In a recent study, Au(III) nano complexes were prepared, showing good biological activity as antioxidants and inhibiting MCF-7 breast cancer cells. The concentrations ranged between 20–120 µg/mL, and the IC_{50} value was 145.27 µg/mL for diseased cells and 192.21 µg/mL for healthy cells [47]. Noor and Kareem [48] prepared an Au(III) complex with a new azo-biphenyl ligand (5-(dimethylamino)-2-(((4-((4,5-diphenyl-)1*H*-imidazol-2-yl)diazenyl)benzyl)imino)methyl)phenol) is a derivative of imidazole. The biological activity of the Au(III) complex was studied in inhibiting MCF-7 cells. Concentrations ranged between 20–100 µg/mL, and the IC_{50} value was 33.92 µg/mL for the diseased cells, while the IC_{50} value was 133.04 µg/mL for healthy cells, where the Au(III) complex proved to be highly efficient in inhibiting the aforementioned type of cancer. In a recent study [49], complexes of some transition elements were prepared with a new azo-Schiff ligand (*N*-(2-(*E*)-(4,5-diphenyl-1*H*-imidazol-2-yl)dibenzyl)-1-(1*H*)indol-3-yl)methanimine) is derived from indole. The toxicological activity of Au(III) complex was studied against the MCF-7 cell line and compared with MCA-10

healthy cells, where it was found to be effective in inhibiting breast cancer cells and safe for healthy cells, Concentrations ranged between 20–100 µg/mL and the IC_{50} value was 36.28 µg/mL for the cancerous cells and 308.35 µg/mL for healthy cells.

Antioxidant Screening

Table 7 shows that compared to other concentrations of produced compounds, the concentration of 200 µg/mL has the highest scavenging activity. The DPPH compound is commonly employed in laboratory settings to assess the efficacy of antioxidants [47-48]. At 517 nm, the compound DPPH exhibits absorption. When DPPH transforms into an antioxidant or a radical, this absorption disappears. The diamagnetic molecule exhibits stability. Consequently, the hue transforms from purple to yellow. The observed shift in hue indicates hydrogen's capacity to provide donations to the compounds being evaluated. Antioxidants can react with DPPH and generate 1.1-diphenyl-2-picryl-hydrazine. Interactions with stable free-standing (1.1-divinyl-2-picryl-hydrazine) over 30 min at five diverse concentrations were used to evaluate the limiting capabilities of the compounds. Electron-withdrawing substituents typically render aromatic rings inactive and unable to bind free radicals. The evaluation of antioxidant activity revealed that all the synthesized compounds possess antioxidant characteristics, as demonstrated by their comparison with established antioxidants such as ascorbic acid [50–54]. This assessment was conducted using the stable free radical method [18].

■ CONCLUSION

In this study, the new ligand L_1 and its complexes of Co(II), Ni(II), nano-complexes of Cu(II), Zn(II), and Au(III) were synthesized and analyzed using standard procedures. Based on theoretical data and spectroscopic analyses, the geometrical shape of Co(II), Ni(II), Cu(II), and Zn(II) metallic complexes was octahedral, while the Au(III) complex was square planar. The L_1 works as a tridentate coordinating agent by coordinating the donor atoms to metal ions, namely through the nitrogen atom of the azomethine group. The nitrogen atom of the NH–CH group belongs to the thiobarbituric acid cycle, and the oxygen atom of the carboxylic group. The results are definite using FTIR spectra and molecular docking was performed tp determine the metal complexes' activity towards the breast cancer protein receptor (1HK7). Furthermore, the results exposed that ligand L_1 exhibited superior antioxidant characteristics in comparison to its metallic complexes. In addition, the nano-complex of Au(III) confirmed significant anticancer activity against MCF-7 cells, with an IC_{50} value of 103.43 µg/mL. This nano-complex of Au(III) has been shown to be effective in cancer cells, while its effect was safe on normal cells. Therefore, this compound can be considered a new therapeutic compound for this type of cancer.

■ ACKNOWLEDGMENTS

The authors would like to express our deep gratitude to the Department of Chemistry at the Faculty of Education for Women, Kufa University, for helping to finish this work. We would like to thank the technical staff at the Central Laboratory of the College of Pharmacy, Kufa University, for providing the necessary technical assistance and support in the experiments.

■ CONFLICT OF INTEREST

The authors do not have a conflict of interest.

■ AUTHOR CONTRIBUTIONS

Thanaa Abdul Ameer Hilal conducted the experiment and wrote the manuscript, and Ibtihal Kadhim Kareem interpreted the results obtained from measurements and revised the manuscript. All authors agreed to the final version of this manuscript.

■ REFERENCES

[1] Dvořák, Z., Poulíková, K., and Mani, S., 2021, Indole scaffolds as a promising class of the aryl hydrocarbon receptor ligands, *Eur. J. Med. Chem.*, 215, 113231.

[2] Jia, Y., Wen, X., Gong, Y., and Wang, X., 2020, Current scenario of indole derivatives with potential anti-drug-resistant cancer activity, *Eur. J. Med. Chem.*, 200, 112359.

[3] Bhakhar, K.A., Sureja, D.K., and Dhameliya, T.M., 2022, Synthetic account of indoles in search of

potential anti-mycobacterial agents: A review and future insights, *J. Mol. Struct.*, 1248, 131522.

[4] Yang, L., Chen, X., Ni, K., Li, Y., Wu, J., Chen, W., Ji, Y., Feng, L., Li, F., and Chen, D., 2020, Proton-exchanged montmorillonite-mediated reactions of hetero-benzyl acetates: Application to the synthesis of Zafirlukast, *Tetrahedron Lett.*, 61 (29), 152123.

[5] Sasmal, P.K., Ramachandran, G., Zhang, Y., and Liu, Z, 2021, First total synthesis of 3a-hydroxy-1,1-dimethyl-5-((*N*-methylsulfamoyl)methyl)-1,2,3,3a,8,8a-hexahydropyrrolo[2,3-b]indol-1-ium 2,2,2-trifluoroacetate by mimicking the oxidative degradation pathway of sumatriptan, *Results Chem.*, 3, 100173.

[6] Dadashpour, S., and Emami, S., 2018, Indole in the target-based design of anti-cancer agents: A versatile scaffold with diverse mechanisms, *Eur. J. Med. Chem.*, 150, 9–29.

[7] Oulmidi, A., Radi, S., Idir, A., Zyad, A., Kabach, I., Nhiri, M., Robeyns, K., Rotaru, A., and Garcia, Y., 2021, Synthesis and cytotoxicity against tumor cells of pincer *N*-heterocyclic ligands and their transition metal complexes, *RSC Adv.*, 11 (55), 34742–34753.

[8] Abbas, H.H., Al-Luaibi, M.Y., and Al-Assadi, M.J., 2023, New heterocyclic organo-chalcogenide compounds: Synthesis, physicochemical characterization, and evaluation of anti-cancer activity against breast cancer cells, *Indones. J. Chem.*, 23 (2), 309–320.

[9] Yasir, A.F., and Jamel, H.O., 2023, Synthesis of a new DPTYEAP ligand and its complexes with their assessments on physical properties, antioxidant, and biological potential to treat breast cancer, *Indones. J. Chem.*, 23 (3), 796–808.

[10] Wei, H.C., 2019, Mathematical modeling of tumor growth: The MCF-7 breast cancer cell line, *Math. Biosci. Eng.*,16 (6), 6512–6535.

[11] Albrand, G., and Terret, C., 2008, Early breast cancer in the elderly, *Drugs Aging*, 25 (1), 35–45.

[12] Kuarm, B.S., Reddy, Y.T., Madhav, J.V., Crooks, P.A., and Rajitha, B., 2011, 3-[Benzimidazo- and 3-[benzothiadiazoleimidazo-(1,2-*c*)quinazolin-5-yl]-2*H*-chromene-2-ones as potent antimicrobial agents, *Bioorg. Med. Chem. Lett.*, 21 (1), 524–527.

[13] Laxmi, S.V., Thirupathi, R.Y, Suresh, K.B., Narsimha, R.P., Crooks, P.A., and Rajitha, B., 2011, Synthesis and evaluation of chromenyl barbiturates and thiobarbiturates as potential antitubercular agents, *Bioorg. Med. Chem. Lett.*, 21 (14), 4329–4331.

[14] Laxmi, S.V., Rajitha, G., Rajitha, B., and Rao, A.J., 2016, Photochemical synthesis and anti-cancer activity of barbituric acid, thiobarbituric acid, thiosemicarbazide, and isoniazid linked to 2-phenyl indole derivatives, *J. Chem. Biol.*, 9 (2), 57–63.

[15] Wang, G., Peng, Z., and Li, Y., 2019, Synthesis, anticancer activity and molecular modeling studies of novel chalcone derivatives containing indole and naphthalene moieties as tubulin polymerization inhibitors, *Chem. Pharm. Bull.*, 67 (7), 725–728.

[16] Rajashakar, V., Saisree, K., Sikender, M., Naveen, S., Madhava Reddy, B., and Harinadha Babu, V., 2016, Synthesis of pyrazolyl thiobarbituric acids and their cytotoxic and antimicrobial evaluation, *Pharma Chem.*, 8 (10), 109–113.

[17] Majeed, H.H., and Abbas, A.F., 2023, Synthesis, characterization and antioxidant activity of Schiff base derivatives from [6,6'-(1,4-phenylene)bis(4-(4-aminophenyl) pyrimidin)], *J. Kufa Chem. Sci.*, 3 (1), 313–344.

[18] Hadi, M.A., and Kareem, I.K., 2020, Synthesis and characterization of some transition metal complexes with new azo-Schiff base ligand 3,4-bis(((1*E*,2*E*)-2-((2-((4-((*Z*)-(3-hydroxyphenyl)diazenyl)naphthalen-1-yl)amino)ethyl)imino)-1,2-diphenylethylidene) amino)phenyl)(phenyl)methanone, *Egypt. J. Chem.*, 63 (1), 301–313.

[19] Mohssen, H.F., Ali, N.M., and Ali, H.A., 2017, Synthesis, characterization and antimicrobial activity of some new heterocyclic compounds from meldrum acid, *J. Chem. Pharm. Res.*, 9 (1), 209–219.

[20] Aljamali, N.M., and Jawad, S.F., 2022, Preparation, spectral characterization, thermal study, and

antifungal assay of (formazane -mefenamic acid)-derivatives, *Egypt. J. Chem.*, 65 (2), 449–457.

[21] Al-adilee, K.J., and Hessoon, H.M., 2019, Synthesis, spectral properties and anticancer studies of novel hetrocyclic azo dye ligand derived from 2-amino-5-methyl thiazole with some transition metal complexes, *J. Phys.: Conf. Ser.*, 1234 (1), 012094.

[22] Imran, W.J., Kareem, I.K., and Jaafar, R.R., 2023, Synthesis and spectral identifications of new azo – Schiff base ligand (4Cl-2DIBP) derived from (para-aminobenzylamine) with its some metallic complexes, *J. Kufa Chem. Sci.*, 2 (10), 1–16.

[23] Sami, S., and Shaalan, N., 2024, Synthesis, structure, and biological activity studies of new metal ion complexes based on 3-[(3-hydroxynaphthalene-2-yl-ethylidene)-hydrazono]-1,3-dihydro-indol-2-one, *Indones. J. Chem*., 24 (2), 370–378.

[24] Kyhoiesh, H.A.K., and Hassan, H.M., 2024, Synthesis, characterization, *in silico* DFT, molecular docking, ADMET profiling studies and toxicity predictions of Ag(I) complex derived from 4-aminoacetophenone, *ChemistrySelect*, 9 (4), e202304429.

[25] Mbarki, F., and Ammari, F., 2021, Chemical modification of commercial and recovered poly(vinyl chloride) with amino groups - Adsorption of heavy metals (Cr(III), Pb(II), Cd(II), or Co(II)) by modified PVC polymers, *J. Maroc. Chim. Heterocycl.*, 20 (2), 80–94.

[26] Ali, I., Said, M.H., and AlWazn, W., 2021, Preparation, characterization, and study of complexes containing beta-lactam group with some transitional elements and their biological activity, *Egypt. J. Chem.*, 64 (10), 5703–5712.

[27] Pahontu, E., Socea, L.I., Barbuceanu, S.F., Ilies, D.C., Badea, M., Olaru, O.T., Gulea, A., Socea, B., and Bratu, O.G., 2018, Synthesis, characterization and toxicity evaluation of Cu(II), Mn(II), Co(II), Ni(II), Pd(II) complexes with ligand derived from hydrazinecarbothioamide, *Rev. Chim.*, 69 (11), 2959–2963.

[28] Radhi, S.M.J., Kareem, I.K., and Majeed, N.S., 2023, Preparation and characterization of new mixed ligand complexes for some transition metal ions (bivalent) with Schiff- Mannich and Schiff base ligands, *J. Kufa Chem. Sci.*, 3 (1), 1–25.

[29] Yahya, W.I., Mgheed, T.H., and Kadhium, A.J., 2022, Preparation, characterization of some metal complexes of new mixed ligands derived from 5-methyl imidazole and study the biological activity of palladium(II) complex as anticancer, *NeuroQuantology*, 20 (1), 71–83.

[30] Jailani, A.K., Gowthaman, N.S.K., and Kesavan, M.P., 2020, Synthesis, characterisation and biological evaluation of tyramine derived Schiff base ligand and its transition metal(II) complexes, *Karbala Int. J. Mod. Sci.*, 6 (2), 15.

[31] El-Gammal, O.A., Mohamed, F.S., Rezk, G.N., and El-Bindary, A.A., 2021, Synthesis, characterization, catalytic, DNA binding and antibacterial activities of Co(II), Ni(II) and Cu(II) complexes with new Schiff base ligand, *J. Mol. Liq.*, 326, 115223.

[32] Kyhoiesh, H.A.K., Al-Hussainawy, M.K., and Saud, H.R., 2022, Synthesis and characterization of polyacrylamide/crotonic acid and its composites with carbon nanotube and Rhodamine B, *AIP Conf. Proc.*, 2398 (1), 030018.

[33] Jaber, S.A., Kyhoiesh, H.A.K., and Jawad, S.H., 2021, Synthesis, characterization and biological activity studies of cadmium(II) complex derived from azo ligand 2-[2′-(5-bromo thiazolyl) azo]-5-dimethyl amino benzoic acid, *J. Phys.: Conf. Ser.*, 1818 (1), 012013.

[34] Al-Hussainawy, M.K., Sahb Mehdi, Z., Jasim, K.K., Alshamsi, H.A., Saud, H.R., and Kyhoiesh, H.A.K., 2022, A single rapid route synthesis of magnetite/chitosan nanocomposite: Competitive study, *Results Chem.*, 4, 100567.

[35] Safont-Sempere, M.M., Fernández, G., and Würthner, F., 2011, Self-sorting phenomena in complex supramolecular systems, *Chem. Rev.*, 111 (9), 5784–5814.

[36] Shenashen, M.A., El-Safty, S.A., and Elshehy, E.A., 2014, Synthesis, morphological control, and properties of silver nanoparticles in potential applications, *Part. Part. Syst. Charact.*, 31 (3), 293–316.

[37] Król, A., Pomastowski, P., Rafińska, K., Railean-Plugaru, V., and Buszewski, B., 2017, Zinc oxide nanoparticles: Synthesis, antiseptic activity and toxicity mechanism, *Adv. Colloid Interface Sci.*, 249, 37–52.

[38] El-Boraey, H.A., and El-Domiaty, A.M., 2021, Influences of γ-ray irradiation on physico-chemical, structural, X-ray diffraction, thermal and antimicrobial activity of some γ-irradiated *N′*,*N‴*-((Z)-ethane-1,2-diylidine)bis(2-aminobenzohydrazide) metal complexes, *Appl. Radiat. Isot.*, 174, 109774.

[39] Marulanda Cardona, D.M., Wongsa-Ngam, J., Jimenez, H., and Langdon, T.G., 2017, Effects on hardness and microstructure of AISI 1020 low carbon steel processed by high-pressure torsion, *J. Mater. Res. Technol.*, 6 (4), 355–360.

[40] Abd Al-Sadda, H.K., Al-Hussainawy, M., and Kyhoiesh H.A.K., 2019, Synthesis, spectral characterization and biological activity of 2-[2¯-(1-amino-1, 5-dinitrophenyl)azo]-imidazole, *J. Global Pharma Technol.*, 11 (7), 165–174.

[41] Mustapha, S., Ndamitso, M.M., Abdulkareem, A.S., Tijani, J.O., Shuaib, D.T., Mohammed, A.K., and Sumaila, A., 2019, Comparative study of crystallite size using Williamson-Hall and Debye-Scherrer plots for ZnO nanoparticles, *Adv. Nat. Sci.: Nanosci. Nanotechnol.*, 10 (4), 450.

[42] Serafińczuk, J., Moszak, K., Pawlaczyk, Ł., Olszewski, W., Pucicki, D., Kudrawiec, R., and Hommel, D., 2020, Determination of dislocation density in GaN/sapphire layers using XRD measurements carried out from the edge of the sample, *J. Alloys Compd.*, 825, 153838.

[43] Kyhoiesh, H.A.K., and Al-Adilee, K.J., 2023, Pt(IV) and Au(III) complexes with tridentate-benzothiazole based ligand: Synthesis, characterization, biological applications (antibacterial, antifungal, antioxidant, anticancer and molecular docking) and DFT calculation, *Inorg. Chim. Acta*, 555, 121598.

[44] El-Sherif, A.A., 2009, Synthesis, spectroscopic characterization and biological activity on newly synthesized copper(II) and nickel(II) complexes incorporating bidentate oxygen–nitrogen hydrazone ligands, *Inorg. Chim. Acta*, 362 (14), 4991–5000.

[45] Zalevskaya, O.A., and Gur'eva, Y.A., 2021, Recent studies on the antimicrobial activity of copper complexes, *Russ. J. Coord. Chem.*, 47 (12), 861–880.

[46] Rudrapal, M., Gogoi, N., Chetia, D., Khan, J., Banwas, S., Alshehri, B., Alaidarous, M.A., Laddha, U.D., Khairnar, S.J., and Walode, S.G., 2022, Repurposing of phytomedicine-derived bioactive compounds with promising anti-SARS-CoV-2 potential: Molecular docking, MD simulation and drug-likeness/ADMET studies, *Saudi J. Biol. Sci.*, 29 (4), 2432–2446.

[47] Redha, M.M., and Mohammed, L.A., 2023, Study of microscopic properties and antioxidant effect of azo ligand, *Tuijin Jishu*, 44 (2), 214–223.

[48] Noor, S.S., and Kareem, I.K., 2024, Exploring the anticancer activity of gold complex with newly ligand (DDIBM): Synthesis, spectral identification and magnetic susceptibility of its metallic complexes, *Indones. J. Chem.*, 24 (3), 822–834.

[49] Kumar Madugula, A., Kiran, B., Suresh Varma Dendukuri, B.N., Kishore, T.V.N., Srinivasa Rao, P., Ranagaih, G., and Jagadeesh, K., 2024, Synthesis, characterization, and evaluation of antioxidant, antimicrobial and drug likeness properties of indole containing 1,3,4-oxadiazoles, *Results Chem.*, 9, 101664.

[50] Matida, J.J., and Abbs Fen Reji, T.F., 2024, Design, structural characterization, biological evaluation and molecular docking studies of methylindole bearing thiocarbamoylpyrazole moieties, *Indian J. Biochem. Biophys.*, 61 (7), 418–429.

[51] Sabah, R., F.Al-Kazazz, A.S.A.F., and Al-Ameri, S.A.H., 2020, Investigation on glucose and levels of Zn and Cu in Sera of Iraqi males addicted on methamphetamine or tramadol, *J. Adv. Sci. Eng. Technol.*, 3 (2), 52–63.

[52] Al-Daffay, R.K.H., and Al-Hamdani, A.A.S., 2022, Synthesis and characterization of some metals complexes with new acidicazo ligand 4-[(2-amino-4-phenylazo)-methyl]-cyclohexane carboxylic acid, *Iraqi J. Sci.*, 63 (8), 3264–3275.

[53] Sabah, R., 2021, Simultaneous HPLC estimation of amphetamine and caffeine abuse drugs in Iraqi human addicts, *J. Adv. Sci. Eng. Technol.*, 4 (1), 25–31.

[54] Mohammed, D., Enouz, A.J., and Areaaer, A.H.J., 2021, Effect of adding different levels of antioxidant and imported ginseng (panax) roots to the diet in the microbial, *Kufa. J. Agric. Sci.*, 13 (2), 1–5.